UNITED NATIONS EDUCATIONAL, SCIENTIFIC AND CULTURAL ORGANIZATION
INTERNATIONAL ATOMIC ENERGY AGENCY
INTERNATIONAL CENTRE FOR THEORETICAL PHYSICS
I.C.T.P., P.O. BOX 586, 34100 TRIESTE, ITALY, CABLE: CENTRATOM TRIESTE

H4.SMR/1013-7

SCHOOL ON THE USE OF SYNCHROTRON RADIATION
IN SCIENCE AND TECHNOLOGY:
"John Fuggle Memorial"

3 November - 5 December 1997

Miramare - Trieste, Italy

Theoretical Aspects of Electron Emission Holography [2)]

Luciano Fonda
ICTP - Trieste, Italy

Review Article

phys. stat. sol. (b) **188**, 599 (1995)

Subject classification: 79.60; 61.14

Department of Theoretical Physics, University of Trieste, and International Center for Theoretical Physics, Trieste[1])

Theoretical Aspects of Electron Emission Holography[2])

By

L. FONDA

Contents

1. *Introduction*

2. *Photoelectron and Auger electron holography*

3. *Elimination of twin images and self-hologram effects in photoelectron holography*

4. *Treatment of angular anisotropies*
   4.1 The SWEEP method
   4.2 The SWIFT method

5. *Conclusions*

References

1. Introduction

Starting from a suggestion of Szöke [1] and Barton [2], a new surface structure determination approach, called either photoelectron or Auger electron holography depending on the process under consideration, to get three-dimensional images of the close vicinity of a given near-surface atom emitter, has recently been developed. The idea goes back to Gabor's discovery of holography [3]. He realized that, by recording on a photographic plate the interference pattern (hologram) of a known *reference* wave with an unknown *object* wave and then illuminating with an appropriate decoding wave the so obtained hologram, one can obtain the image of the object.

In the case of a photoelectron or of an Auger electron, the reference wave is assumed to be the direct wave emitted by the excited atom a. The object wave is then the superposition of the waves emitted coherently by the atoms surrounding a as a consequence of the process of single double ... multiple scattering experienced by the emitted electron. By taking the detector to be a spherical photographic film, the decoding wave referred to above is then chosen to be the spherical wave, converging on the film, obtained from the asymptotic reference wave via the operation of time reversal [1, 2]. This wave is transmitted through

[1]) POB 586, Strada Costiera 11, I-34100 Trieste, Italy.

[2]) Supported in part by the Istituto Nazionale Fisica Nucleare.

the film and in this process it collects the information contained in the hologram. The images of the atoms of the object are then obtained by means of computer reconstruction using a mathematical method similar to the one employed in optical holography.

In this way, one therefore realizes the inverse process of recovering the structure of the object from the knowledge of the hologram.

The advantage of this holographic method lies in the knowledge of the reference wave, a point which is not shared by structure determination approaches using an external beam of particles, such as e.g. X-ray and neutron diffractions, where the reference wave is lost and the experimentalist is therefore faced with the so-called "phase problem".

In Section 2, the theory of electron emission holography is expounded in full detail. In Sections 3 and 4, the weak points of the theory, such as the appearance of twin images, of "ghost atoms", and of some other artificial byproducts of the method, are discussed and ways to eliminate them are reviewed.

Applications of this holographic technique have appeared in the literature. For a complete list of references, the reader is referred to the review papers by Chambers [4] and Fadley [5].

2. Photoelectron and Auger Electron Holography

Let us first consider the way the hologram is obtained. We place a spherical photographic film around our object. The centre of the sphere is at the origin 0 of the reference frame placed at the centre of the atom emitter a. The radius of the sphere is R. Each point of the film is characterized by the polar angles defining the vector $\boldsymbol{R}$.

The interference pattern is encoded on this photographic film. It is obtained by evaluating the component of the emitted electron vector probability current density in the direction perpendicular to the sphere surface (for simplicity, we neglect the refraction of the electron wave at the surface of the sample subject to measurement),

$$I(\boldsymbol{R}) \equiv \boldsymbol{j}(\boldsymbol{R}) \cdot \boldsymbol{R}/R \,. \tag{2.1}$$

If the detector is in the far field (R large with respect to the dimensions of the object), this probability is just proportional to the modulus square of the emitted electron wave function $\psi(\boldsymbol{R})$ evaluated at the position $\boldsymbol{R}$,

$$I(\boldsymbol{R}) \propto |\psi(\boldsymbol{R})|^2 \,. \tag{2.2}$$

On the sphere surface the wave function $\psi(\boldsymbol{R})$ can be expressed in terms of the scattering matrix

$$\psi(\boldsymbol{R})_{R\,\text{large}} \approx -\frac{m(2\pi)^{1/2}}{\hbar^2}\,\frac{e^{ikR}}{R}\,T_{f-i} \,. \tag{2.3}$$

T_{f-i} is the T-matrix for the process evaluated on the energy shell. In the standard single-particle approach, it is given by

$$T_{f-i} \equiv \langle \psi_f^{(-)}(\boldsymbol{k}) \,|\, A_c \rangle \,, \tag{2.4}$$

where the PhotoElectron state vector $|A_c^{\text{PhE}}\rangle$ and the Auger $|A_{c12}^{\text{Auger}}\rangle$ are defined by (see [6], Sections 2 and 6)

$$|A_c^{\text{PhE}}\rangle = \langle 0|\, H_I \,|1_i\rangle\, |\psi_c\rangle \,, \tag{2.5a}$$

$$\langle r_2 \,|\, A_{c12}^{\text{Auger}}\rangle = \int \mathrm{d}^3 r_1\, \psi_c^*(r_1)\, \frac{e^2}{|r_2 - r_1|}\, [\psi_{i1}(r_1)\, \psi_{i2}(r_2) - \psi_{i2}(r_1)\, \psi_{i1}(r_2)] \,. \tag{2.5b}$$

In the case of photoemission, the initial state vector is the product of the incoming free photon state vector $|1_i\rangle$ (the subscript i symbolizes the initial photon momentum and the polarization) times the vector $|\psi_c\rangle$ which represents the initial single-electron normalized bound state relative to the *core* level c. The final state is given by the product of the normalized photon vacuum $|0\rangle$ times the single-electron scattering state $|\psi_f^{(-)}(k)\rangle$, satisfying an incoming wave boundary condition, describing the emitted electron, with asymptotic momentum $\hbar k \equiv \hbar k R/R$, in interaction with the ionized atom emitter a and with its neighbours in the condensed material. For simplicity, in this paper we shall forget about the spin of the emitted electron. To the first order in the radiation field, the interaction Hamiltonian is given by: $H_1 = -(e/mc)\, A \cdot p$, where m and p are the electron mass and momentum operator, respectively, and $A(r)$ is the quantized photon field in the Coulomb gauge $\nabla \cdot A(r) = 0$.

In the case of Auger emission, the process is one in which an electron of the ionized atom a makes a transition from the core level 1 (core level 2) to the empty core level c, while an electron from the core level 2 (core level 1) is ejected from the atom a. This emitted Auger electron, represented in (2.4) by the usual scattering state $|\psi_f^{(-)}(k)\rangle$, propagates then in the material and suffers multiple scatterings from the atoms surrounding the doubly ionized atom a until, after having finally assumed the momentum $\hbar k$, it reaches the detector.

The expression of the T-matrix in terms of all multiple scatterings is known from the literature. We write here (3.37) of [6] (L is a combined orbital angular momentum index $L \equiv l, m$),

$$T_{f\leftarrow i} = \sum_L \mathcal{T}_L \mathcal{M}_{cL}\,, \tag{2.6a}$$

$$\mathcal{T}_L = \sum_{L'} (2\pi)^{-3/2} (-i)^{l'} Y_{L'}(k) \times \left\{ \delta_{LL'} + \sum_{\substack{p\neq a \\ q=a}} \sum_{L_p L_q} [\delta_{L'L_q} e^{ik\cdot R_{aq}} + t^a_{l'} g_{L'L_q}(R_{aq})]\, \tau^{qp}_{L_q L_p} g_{L_p L}(R_{pa}) \right\}. \tag{2.6b}$$

Apart from the consideration of inelasticities and thermal vibrations, to be introduced with proper attenuation factors [5]. (2.6) is, within the single-particle framework, the correct T-matrix.

The matrix $\tau^{qp}_{L_q L_p}$ is the representative in angular momentum space of the scattering path operator [7]. The integral equation defining this operator is given by (3.38) of [6],

$$\tau^{qp}_{L_q L_p} = t^p_{l_p} \delta_{qp} \delta_{L_q L_p} + \sum_{m\neq q} \sum_{L_m} t^q_{l_q} [g_{L_q L_m}(R_{qm})]\, \tau^{mp}_{L_m L_p}\,, \tag{2.7}$$

$R_{qp} = R_q - R_p$ is the bond vector pointing from atom p to atom q, $t^p_l = -e^{i\delta^p_l} \sin \delta^p_l$ is the l-th wave T-matrix for scattering of the electron from the atom p, the form factor $\mathcal{M}_{cL}$ is given by

$$\mathcal{M}_{cL} = \int d^3r \frac{\psi^{(+)}_{al}(k, r)}{kr} Y^*_L(r) \langle r \mid A_c \rangle\,, \tag{2.8}$$

where $\psi^{(+)}_{al}(k, r)$ is the physical radial scattering wave function, satisfying an outgoing wave boundary condition, belonging to the angular momentum l, for the emitted electron in the field of the potential U_a of the atom emitter a.

The g-propagator (structure factor) is given by

$$g_{L_pL_q}(R_{pq}) = -i \sum_L 4\pi i^{l+l_p-l_q} \langle Y_{L_p} Y_L \mid Y_{L_q} \rangle Y_L(R_{pq})\, h_l^{(+)}(kR_{pq}) . \tag{2.9}$$

Using (2.3), (2.6), and (2.7), we can easily split the wave function, at the sphere surface, into *reference* and *object* terms,

$$\psi(R) = \psi_{\text{ref}}(R) + \psi_{\text{obj}}(R) \equiv -\frac{m(2\pi)^{1/2}}{\hbar^2} \frac{e^{ikR}}{R} \sum_L [\mathscr{T}_L^{\text{ref}} + \mathscr{T}_L^{\text{obj}}] \mathscr{A}_{cL} , \tag{2.10a}$$

$$\mathscr{T}_L^{\text{ref}} = (2\pi)^{-3/2} (-i)^l Y_L(k) , \tag{2.10b}$$

$$\mathscr{T}_L^{\text{obj}} = (2\pi)^{-3/2} \sum_{p,q} \sum_{L_pL_q} (-i)^{l_q} Y_{L_q}(k)\, e^{ik\cdot R_{aq}}\, \tau^{qp}_{L_qL_p} (1 - \delta_{pa})\, g_{L_pL}(R_{pa}) . \tag{2.10c}$$

Note that the object wave contains also all waves which, after having undergone multiple scattering, have atom a as the last scatterer (term $q = a$ of (2.10c)). These particular multiple-scattering contributions are unknown and therefore, even though consisting of waves eventually outgoing from the atom emitter, cannot be included in the reference wave. They are at least of second order with respect to the latter wave.

To decode the information contained in the interference pattern appearing on the spherical film, we imagine to illuminate the film with a converging spherical wave

$$\psi_{\text{decoding}}(r) = \frac{e^{-ikr}}{r} ; \qquad r > R \tag{2.11}$$

obtained, apart from a constant, from the asymptotic expression of the reference wave via the operation of time reversal. This converging wave is transmitted through the film. We suppose that the interference pattern $I(R)$ is imprinted on a positive photographic film which, by proper development, has the contrast value $\gamma = 2$ [8]. As a consequence, the transmittance is linearly related to the intensity $I(R)$ measured on the film and the *transmitted wave* ψ_T on the internal side of the surface of the sphere is therefore given by:

$$\psi_T(R) = (1 + CI(R)) \frac{e^{-ikR}}{R} . \tag{2.12}$$

The transmitted wave satisfies the Helmholtz wave equation

$$(\Delta + k^2)\, \psi_T(r) = -4\pi C_0 \delta^3(r) ; \qquad r \leqq R \tag{2.13}$$

subject to the (Dirichelet) boundary condition (2.12) on the surface of the sphere. $\psi_T(r)$ is singular in the origin $r = 0$ (position of the atom emitter a). This can be understood from the fact that, if there is no hologram ($I = 0$), ψ_T must coincide with the decoding wave (2.11) which satisfies (2.13) with $C_0 = 1$.

In order to find ψ_T in a given point P_0 (of coordinate vector r_0) inside the sphere, we consider the Green's function $K(r \mid r_0)$ satisfying the Helmholtz equation,

$$(\Delta + k^2)\, K(r \mid r_0) = -4\pi \delta^3(r - r_0) \tag{2.14}$$

with boundary condition to be specified in a moment.

We multiply (2.13) by $K(r \mid r_0)$ and (2.14) by $\psi_T(r)$ and subtract member by member one equation from the other. We integrate the so obtained expression on the whole volume of the sphere. Using then the Green's theorem, we get

$$\psi_T(r_0) - C_0 K(0 \mid r_0) = \frac{1}{4\pi} \int [K(r \mid r_0)\, \Delta\psi_T(r) - \psi_T(r)\, \Delta K(r \mid r_0)]\, dV$$

$$= \frac{1}{4\pi} \int \left[\psi_T(r) \frac{\partial K(r \mid r_0)}{\partial n} - K(r \mid r_0) \frac{\partial \psi_T(r)}{\partial n} \right]_{r=R} dS\,, \quad (2.15)$$

where ∂n is the normal to the surface directed into the interior of the sphere.

A natural choice for the Green's function would be [2, 9]: $K(r \mid r_0) = (\exp ik\,|r - r_0|)/|r - r_0|$. In that case, however, from (2.15) we see that knowledge of ψ_T and $\partial\psi_T/\partial n$ on the whole surface should be required to solve our problem. Apart from the fact that on the boundary we know only the values of ψ_T (from (2.12)), this might lead to the following mathematical contradiction: In practice the hologram can cover at most the 2π-hemisphere hanging over the sample subject to measurement; if symmetry arguments are not available in order to obtain mathematically the hologram on the "opaque" sides of the measuring apparatus, one usually assumes the vanishing of the surface integral (2.15) just on those opaque parts of the surface, which implies $\psi_T = \partial\psi_T/\partial n = 0$ there; but this implies, by a well-known theorem, that ψ_T vanishes identically in the whole space.

I shall require that the Green's function vanishes on the boundary surface,

$$K(R \mid r_0) = 0 \quad (2.16)$$

so that (2.15) can be rewritten as

$$\psi_T(r_0) = C_0 K(0 \mid r_0) + \frac{1}{4\pi} \int_S \psi_T(R) \left. \frac{\partial K(r \mid r_0)}{\partial n} \right|_{r=R} dS\,. \quad (2.17)$$

We see that only the knowledge of ψ_T on the boundary is now required.

The integral on the right-hand side of (2.17) may extend now only on the portion S of the surface on which the hologram is actually measured. On the "opaque" parts of the surface we can safely place $\psi_T = 0$ without meeting contradictions of any sort.

We must now solve the Dirichlet boundary value problem posed by (2.14) and (2.16). The solution in the whole space can be found only by means of computer calculations. In fact, for the Helmholtz equation (2.14) an analytic solution satisfying (2.16) cannot be written down. Fortunately, however, we need only to know $\partial K/\partial n$ on the surface of the sphere. In order to find it there explicitly, I shall make a variation of the well-known method of images. This method has been invented for the case of a flat boundary [10]. Let us see which changes are needed for our curved boundary.

Suppose I want to find the value of $\partial K/\partial n$ in a given point $P_s \subset S$. I draw, through the point P_s, the plane T tangent to the surface S. I perform then the space reflection with respect to T and find the image of P_0 (see Fig. 1). Call this new point P_0^*, whose position vector is r_0^*. Consider now the auxiliary Green's function:

$$\tilde{K}(r \mid r_0) = \frac{e^{ikr_1}}{r_1} - \frac{e^{ikr_2}}{r_2}\,, \quad (2.18)$$

where $r_1 = r - r_0$ and $r_2 = r - r_0^*$. In the interior of the sphere, $\tilde{K}$ satisfies the Helmholtz equation (2.14) and it vanishes on the plane T (where $r_1 = r_2$), in particular in the point P_s.

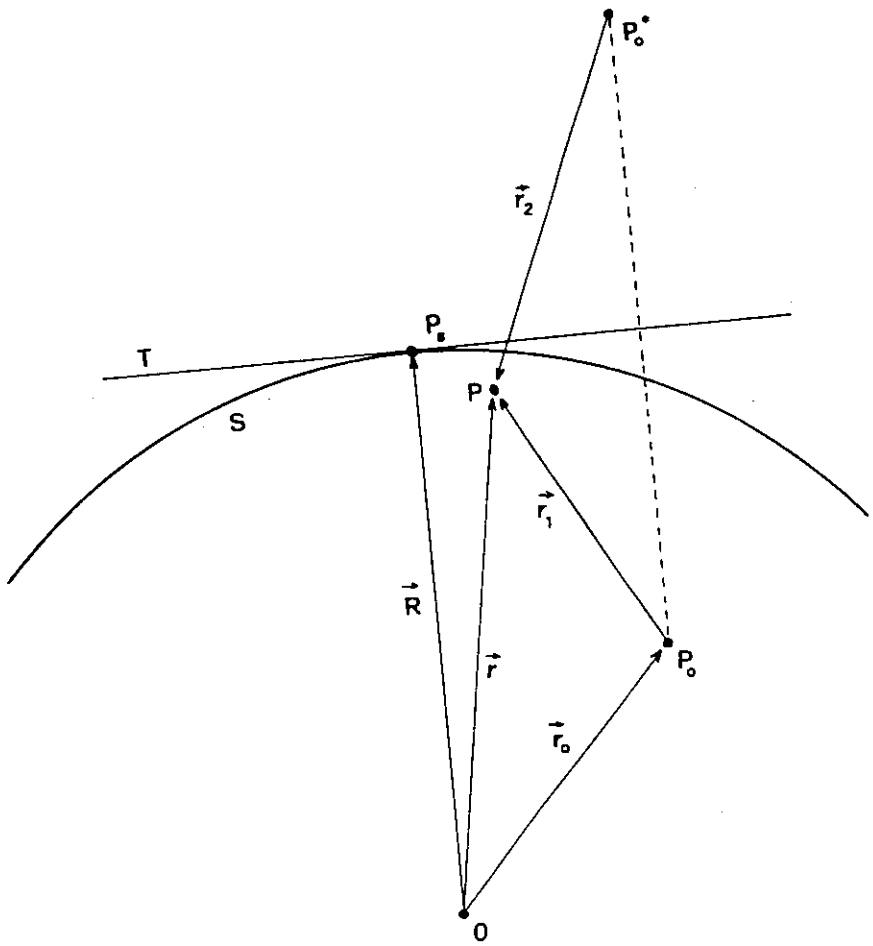

Fig. 1. Definition of points and vectors relative to the construction of the derivative of the Green's function with respect to the normal to the boundary surface

By construction, in any infinitesimal spherical neighbourhood of P_s, the Green's functions K and $\tilde{K}$ differ by infinitesimal quantities and the same holds for their derivatives. We obtain then

$$\left.\frac{\partial K(r \mid r_0)}{\partial n}\right|_{P=P_s} = \left.\frac{\partial \tilde{K}(r \mid r_0)}{\partial n}\right|_{P=P_s}$$

$$= \left[\left(ik - \frac{1}{r_1}\right)\frac{e^{ikr_1}}{r_1}\frac{\partial r_1}{\partial n} - \left(ik - \frac{1}{r_2}\right)\frac{e^{ikr_2}}{r_2}\frac{\partial r_2}{\partial n}\right]_{P=P_s}. \tag{2.19}$$

The evaluation of the derivatives $\partial r_1/\partial n$ and $\partial r_2/\partial n$ in the point P_s is straightforward under the consideration that r_0 is a typical vector spanning the object. Since holography is a short-range order probe ($r_0 < 1.5$ to 2.0 nm) we have that $r_0 \ll R$ and $r_0^* \approx 2R$. Indicating by $\boldsymbol{R}$ the position vector of P_s, we get

$$\left.\frac{\partial r_1}{\partial n}\right|_{P=P_s} \equiv -\frac{\partial |\boldsymbol{R} - \boldsymbol{r}_0|}{\partial R} = -\frac{R - (\boldsymbol{r}_0 \cdot \boldsymbol{R}/R)}{|\boldsymbol{R} - \boldsymbol{r}_0|} \underset{r_0 \ll R}{=} -1\,, \tag{2.20a}$$

$$\left.\frac{\partial r_2}{\partial n}\right|_{P=P_s} \equiv -\frac{\partial |\boldsymbol{R} - \boldsymbol{r}_0^*|}{\partial R} = -\frac{R - (\boldsymbol{r}_0^* \cdot \boldsymbol{R}/R)}{|\boldsymbol{R} - \boldsymbol{r}_0^*|} \underset{r_0^* \approx 2R}{=} +1\,. \tag{2.20b}$$

We therefore obtain

$$\left.\frac{\partial K(r \mid r_0)}{\partial n}\right|_{P=P_s} = -2\left(ik - \frac{1}{r_1}\right)\frac{e^{ikr_1}}{r_1}\bigg|_{P=P_s} \underset{kR \gg 1}{=} -2ik\frac{e^{ik|R-r_0|}}{|R-r_0|}; \qquad r_0 \ll R, \quad (2.21)$$

where we have dropped a term of the order $(kR)^{-1}$ since $kR \gg 1$ (kR is 10^8 to 10^9 in our case).

Using again the smallness of r_0, on the right-hand side of (2.21) for $|R - r_0|$ we can substitute R in the denominator and $R - (R \cdot r_0/R)$ in the exponent. We finally get

$$\frac{\partial K(R \mid r_0)}{\partial n} = -2ik\frac{e^{ikR}}{R}e^{-ik\cdot r_0}; \qquad r_0 \ll R, \quad (2.22)$$

where $k \equiv kR/R$. Using (2.12) and (2.22), and writing $dS \equiv R^2\, d\Omega_k$, (2.17) finally reads

$$\psi_T(r_0) = A_0 + A_1 \int_S d\Omega_k\, I(k)\, e^{-ik\cdot r_0}, \quad (2.23)$$

where $A_0 = C_0 K(0 \mid r_0) - (ik/2\pi)\int_S d\Omega_k\, e^{-ik\cdot r_0}$, $A_1 = -ikC/2\pi$, and $I(k) \equiv I(R)$. A_0 constitutes an uninteresting background; as a function of r_0 it may peak only at the position $r_0 = 0$ of the atom emitter a. Therefore we shall drop it in what follows.

Since all quantities on the right-hand side of (2.23) are known, the wave function $\psi_T(r_0)$ is therefore determined. In the literature, (2.23) is referred to as the Helmholtz-Kirchhoff integral.

Now, also for ψ_T we define *reference* and *object* terms,

$$\psi_T = \psi_{T\,ref} + \psi_{T\,obj}. \quad (2.24)$$

Using (2.2), (2.10a), and (2.23) we get

$$\psi_{T\,ref}(r_0) = A\int_S d\Omega_k\, |\psi_{ref}(R)|^2\, e^{-ik\cdot r_0}, \quad (2.25a)$$

$$\psi_{T\,obj}(r_0) = A\int_S d\Omega_k[\psi^*_{obj}(R)\,\psi_{ref}(R) + \psi_{obj}(R)\,\psi^*_{ref}(R) + |\psi_{obj}(R)|^2]\, e^{-ik\cdot r_0}. \quad (2.25b)$$

The function appearing in the integral (2.25b):

$$\chi(k) \equiv |\psi(R)|^2 - |\psi_{ref}(R)|^2 = \psi^*_{obj}(R)\,\psi_{ref}(R) + \psi_{obj}(R)\,\psi^*_{ref}(R) + \psi^*_{obj}(R)\,\psi_{obj}(R) \quad (2.26)$$

is termed *anisotropy* in the literature. It must be obtained experimentally via subtraction of the reference wave flux. The reference flux is calculated theoretically. One must evaluate carefully the matrix elements $\mathcal{M}_{cL}$ given by (2.8). In the case of photoemission, the dipole excitation of an initial l-wave subshell leads to the interfering $l + 1$ and $l - 1$ final orbital angular momentum channels. The case of Auger emission is much more complex: in practical calculations it is often assumed that the initial state has an s-wave character [4, 5, 11].

Equation (2.25b) is the relevant integral to be evaluated in order to get the image of our object. It transforms the two-dimensional hologram into a three-dimensional image. The first two terms of the integral on the right-hand side of (2.25b) contain the usual hologram of optical holography, while the third term represents the self-interference or self-hologram.

From (2.10), the reference and object waves can be written as

$$\psi_{\mathrm{ref}}(\boldsymbol{R}) = \sum_{L} \mathrm{Y}_{L}(\boldsymbol{k})\, A_{L}\,, \tag{2.27a}$$

$$\psi_{\mathrm{obj}}(\boldsymbol{R}) = \sum_{q} \sum_{L_q} \mathrm{Y}_{L_q}(\boldsymbol{k})\, \mathrm{e}^{\mathrm{i}\boldsymbol{k}\cdot\boldsymbol{R}_{aq}}\, B^{q}_{L_q}\,. \tag{2.27b}$$

Using (2.25b) and (2.27), from a stationary-phase argument [2] we expect that $\psi_{\mathrm{T\,obj}}(r_0)$ will yield peaks at

$$r_0 = \pm \boldsymbol{R}_{aq}\,, \tag{2.28a}$$

$$r_0 = \boldsymbol{R}_{q} - \boldsymbol{R}_{p}\,. \tag{2.28b}$$

This is certainly correct for s-waves (as in the optical case, where s-wave scattering dominates), or in the case of s-wave emission combined with moderately angle dependent scatterings from the neighbours. The latter condition is better realized at low energies since electron scattering presents a high angular anisotropy and relevant phase shifts as the energy increases. As a consequence, artifacts, such as shifts of the position of the atoms and image asymmetry or broadening, appear in the Helmholtz-Kirchhoff integral (2.25b). In Section 4 we shall discuss possible ways to cure these unpleasant features.

In (2.28a), the minus sign is related to the peaks present in the first term of the Helmholtz-Kirchhoff integral (2.25b) and it corresponds to the real images of the atoms of the object; the plus sign corresponds to their twin images. For q = a one gets the image (twin = real) of the atom emitter. The presence of both real and twin images is a problem shared with optical holography.

The uncertainty principle of course limits the ultimate resolution with which the positions of the atoms can be determined by this method [20, 4, 5]: $\Delta r \geqq 1/(k_{\max} - k_{\min})$, where the projections of $\hbar(k_{\max} - k_{\min})$ on the coordinate axes are the uncertainties on the measured electron momenta.

If one centres the relevant part of the hologram along the z-axis and calls θ the half opening angle of the corresponding cone, the Heisenberg principle yields $\Delta x = \Delta y = \pi/(k \sin\theta) = \lambda_{\mathrm{c}}/(2 \sin\theta)$ and $\Delta z = 2\pi/[k(1 - \cos\theta)] = \lambda_{\mathrm{c}}/(1 - \cos\theta)$ showing that the resolution of the images of the atoms should improve for wider θ (with upper limit $\pi/2$) and using higher energy electrons.[3])

Equation (2.28b) corresponds to the third term of (2.25b) and yields peaks at the $\pm$ interdistances of all pairs of atoms, as an expression of the self-hologram; for $q = p$ one gets peaks at $r_0 = 0$, i.e. at the position of the atom emitter a, which after all is not too bad, but, more importantly, for $q \neq p$ peaks appear at positions where there are no atoms. These *ghost* images, which actually appear to be 10 to 20% in size of the real and twin

[3]) For $\theta = 60°$, at the electron energy of 100 eV one gets $\Delta x = \Delta y = 0.071$ nm, $\Delta z = 0.25$ nm. At 1000 eV: $\Delta x = \Delta y = 0.022$ nm, $\Delta z = 0.076$ nm.

images [12], would not be there if the holographic requirement $|\psi_{\mathrm{ref}}| \gg |\psi_{\mathrm{obj}}|$ were satisfied, as it happens in the simpler optical case. In the photoelectron or Auger electron holography this is not so since the electron–atom interaction is in general stronger, particularly for scattering in forward directions along a chain of atoms at high energies.

We shall see in Section 3 how one can eliminate the twin images and the noise due to the self-hologram in the case of photoelectrons.

We end this section by pointing out that the holographic method has the potential of getting information on near-surface atoms beyond nearest neighbours [4, 5], something which is not obtainable by the photoelectron or Auger electron diffraction approaches.

Methods of the type discussed in this section can also be applied to core level X-ray fluorescence [1, 13], to DLEED (diffuse low-energy electron diffraction) [14], and to Kikuchi patterns [15]. Spin-polarized photoelectron holography has been treated in [16, 17].

3. Elimination of Twin Images and Self-Hologram Effects in Photoelectron Holography

We shall treat in this section a method devised to cope with unphysical artifacts such as twin images and self-hologram effects in photoelectron holography.

The method suggested by Barton, Tong, and coworkers [18 to 23] introduces a Fourier transform operation in energy on $\psi_{\mathrm{Tobj}}(r_0)$. In order to see this in detail, let us first apply the plane wave approximation (PWA) to our formulas. This approximation is able to render explicit the energy dependence of the propagators. It consists in fact in replacing, in the g-propagator, the Hankel function $h_l^{(+)}(kR)$ with its expression for large kR: $(-i)^{l+1}\, e^{ikR}/kR$.

For the g-propagator one then obtains

$$(g_{L_pL_q}(R_{pq}))_{\mathrm{PWA}} = -\frac{4\pi}{k}\, i^{l_p - l_q} Y^*_{L_p}(R_{pq})\, \frac{e^{ikR_{qp}}}{R_{pq}}\, Y_{L_q}(R_{pq})\,. \tag{3.1}$$

We finally get the PWA expression of the object part of the wave function

$$\{\psi_{\mathrm{obj}}(R)\}_{\mathrm{PWA}} = -\frac{m}{2\pi\hbar^2}\, \frac{e^{ikR}}{R} \sum_L i^l c_L \sum_{\substack{p \neq a \\ q}} e^{ikr_{aq}} F^{\mathrm{PWA}}_{qp}(k_{rq}; k_{pa})\, \frac{e^{ikR_{pa}}}{R_{pa}}\, (-i)^l\, Y_L(R_{pa})\,, \tag{3.2}$$

where the multiple scattering amplitude $F^{\mathrm{PWA}}_{qp}(k_{xq}; k_{pa})$ is defined by (see [6], Section 4).

$$F^{\mathrm{PWA}}_{qp}(k_{xq}; k_{pa}) = -\frac{4\pi}{k} \sum_{L_pL_q} i^{l_p - l_q} Y_{L_q}(k_{xq})\, (\tau^{qp}_{L_qL_p})_{\mathrm{PWA}}\, Y^*_{L_p}(k_{pa})\,. \tag{3.3}$$

In terms of the scattering factor (scattering amplitude) f_p it satisfies the following multiple-scattering matrix equation:

$$F^{\mathrm{PWA}}_{qp}(k_{xq}; k_{pa}) = \delta_{qp} f_p(k_{xp}; k_{pa}) + \sum_m f_q(k_{xq}; k_{qm})\, \frac{e^{ikR_{qm}}}{R_{qm}}\, (1 - \delta_{qm})\, F^{\mathrm{PWA}}_{mp}(k_{qm}; k_{pa}) \tag{3.4}$$

with its perturbation expansion[4])

$$F_{qp}^{\mathrm{PWA}}(k_{xq}; k_{pa}) = \delta_{qp} f_p(k_{xp}; k_{pa}) + f_q(k_{xq}; k_{qp}) \frac{e^{ikR_{qp}}}{R_{qp}} (1 - \delta_{qp}) f_p(k_{qp}; k_{pa})$$
$$+ \sum_m f_q(k_{xq}; k_{qm}) \frac{e^{ikR_{qm}}}{R_{qm}} (1 - \delta_{qm}) f_m(k_{qm}; k_{mp}) \frac{e^{ikR_{mp}}}{R_{mp}} (1 - \delta_{mp})$$
$$\times f_p(k_{mp}; k_{pa}) + \dots . \tag{3.5}$$

Let us now discuss the general structure, as far as the energy dependence of the propagators is concerned, of the terms appearing under the sign of integration of the Helmholtz-Kirchhoff integral (2.25b). For the first term, using (3.2) and (3.5), we can write

$$\int_S d\Omega_k \, e^{-ik \cdot r_0} \{\psi_{\mathrm{obj}}^*(R) \, \psi_{\mathrm{ref}}(R)\}_{\mathrm{PWA}}$$

$$= \int_S d\Omega_k \, e^{-ik \cdot r_0} \left\{ \sum_q M_q^* \, e^{-ik \cdot R_{aq}} \frac{e^{-ikR_{qa}}}{R_{qa}} (1 - \delta_{qa}) \right.$$

$$+ \sum_{q,p} M_{qp}^* \, e^{-ik \cdot R_{aq}} \frac{e^{-ikR_{qp}}}{R_{qp}} (1 - \delta_{qp}) \frac{e^{-ikR_{pa}}}{R_{pa}} (1 - \delta_{pa})$$

$$\left. + \sum_{q,p,m} M_{qpm}^* \, e^{-ik \cdot R_{aq}} \frac{e^{-ikR_{qp}}}{R_{qp}} (1 - \delta_{qp}) \frac{e^{-ikR_{pm}}}{R_{pm}} (1 - \delta_{pm}) \frac{e^{-ikR_{ma}}}{R_{ma}} (1 - \delta_{ma}) + \dots \right\} . \tag{3.6}$$

As suggested in [18 to 23], we now take the following energy Fourier transform on the Helmholtz-Kirchhoff integral (2.25b):

$$\psi'_{\mathrm{Tobj}}(r_0) = \int_0^{+\infty} \{\psi_{\mathrm{Tobj}}(r_0)\}_{\mathrm{PWA}} \, e^{ikr_0} \, w(k) \, dk , \tag{3.7}$$

$w(k)$ is a proper weight function which can limit the integration interval. It could be a sum of Dirac δ-functions.

After application of the Fourier transform (3.7) to (3.6), we discover that, apart from particular cases which we shall discuss in a while, we are able to get the suppression of all but the first term on the right-hand side (which represents the single-scattering contributions from the neighbours of the atom a (note that $q \neq a$)): For this term in fact, the peaks which appear at the real positions of the atoms $r_0 = R_{qa} \equiv R_q - R_a$ after integrating over angles, get reinforced after the energy Fourier transform (3.7) is performed, as can be understood from the stationary phase argument applied to the phase factor $\exp[ik(r_0 - R_{qa})]$. On the

[4]) $f_q(k_{xq}; k_{qp}) \equiv f_q(\theta_{xqp})$ is the scattering factor describing the electron as being shot from the atom p, scattering from the atom q, and emerging in the direction x (θ_{xqp} is the corresponding polar angle of scattering). For the differential cross section one has: $d\sigma/d\Omega = |f(\theta)|^2$. The scattering factor is connected with the partial wave T-matrix as follows: $f_q(\theta) = -(4\pi/k) \sum_L Y_L^*(k) \, t_l^q Y_L(k')$. (Note that formulae like (3.5) must be read from right to left in order to follow the correct time arrow of the process.)

contrary, the other, multiple-scattering, terms of (3.6) are in general suppressed, since the peak resulting from the energy integration does not coincide with that obtained from the angular integration.

As mentioned above, there are, however, particular cases where multiple scatterings contribute.

Consider for example the second term of (3.6). The angular integral peaks again at $r_0 = R_{qa} \equiv R_q - R_a$. When its Fourier transform (3.7) is taken, the energy phase factor $\exp[ik(r_0 - R_{qp} - R_{pa})]$ will give a contribution if the atom p is aligned with q and atom a so that $R_{qp} + R_{pa} = R_{qa}$ (i.e. p lies in between a and q), since in this way the peaks resulting from angular and energy integrations coincide. The contribution of this a pq chain will then add up to the q-term of the first term of (3.6). Similar considerations hold for the other terms of (3.6) which contribute if chains a $jk \ldots pq$ of aligned atoms are realized so that $R_{qp} + \ldots + R_{kj} + R_{ja} = R_{qa}$.

However, the contribution of these multiple scatterings is not harmful since it enhances the single-scattering term corresponding to the end atom of the chain.

Another possibility, which we have already mentioned in Section 2, is the case q = a which yields a peak at the position $r_0 = 0$. It represents the image (true = twin) of the atom emitter, and it appears at least as a second-order effect.

Let us now consider the second term of the Helmholtz-Kirchhoff integral (2.25b),

$$\int_S d\Omega_k \, e^{-ik\cdot r_0} \{\psi_{obj}(R)\, \psi^*_{ref}(R)\}_{PWA}$$

$$= \int_S d\Omega_k \, e^{-ik\cdot r_0} \left\{ \sum_q M_q \, e^{ik\cdot R_{aq}} \frac{e^{ikR_{aq}}}{R_{qa}} (1 - \delta_{qa}) \right.$$

$$\left. + \sum_{q,p} M_{qp} \, e^{ik\cdot R_{aq}} \frac{e^{ikR_{qp}}}{R_{qp}} (1 - \delta_{qp}) \frac{e^{ikR_{pa}}}{R_{pa}} (1 - \delta_{pa}) + \ldots \right\}. \tag{3.8}$$

The angular integration yields the twin images of the atoms of the object, at the positions $r_0 = -R_{qa} \equiv R_a - R_q$, space reflected of the positions of the true images. However, the Fourier transform (3.7) of expression (3.8) suppresses all the terms since the energy phase factors $\exp(ik(r_0 + R_{qa}))$ $(q \neq a)$ or $\exp(ik(r_0 + R_{qp} + \ldots + R_{ja}))$ are always highly oscillating whichever the positions of the atoms. At most, a little contribution to the "background" bump at the position $r_0 = 0$ of the emitter is obtained.

The purpose of eliminating the twin images has therefore been achieved.

We come now to the discussion of the third (self-hologram) term of (2.25b). Its energy Fourier transform is

$$\int_0^{+\infty} dk \, w(k) \, e^{ikr_0} \int_S d\Omega_k \, e^{-ik\cdot r_0} \{|\psi_{obj}(R)|^2\}_{PWA}$$

$$= \int_0^{+\infty} dk \, w(k) \, e^{ikr_0} \int_S d\Omega_k \, e^{-ik\cdot r_0} \left\{ \sum_{p,q} H_{qp} \, e^{ik\cdot(R_{ap} - R_{aq})} \frac{e^{ik(R_{pa} - R_{qa})}}{R_{pa} R_{qa}} (1 - \delta_{pa})(1 - \delta_{qa}) \right.$$

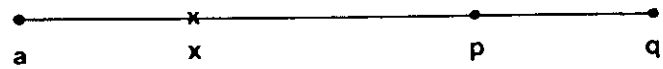

Fig. 2. After Fourier transform on the energy, in the self-hologram there still appear false atom (ghost) images along forward scattering chains of at least three atoms

$$+ \sum_{n,p,q} \left[H_{qpn} \, e^{ik \cdot (R_{ap} - R_{aq})} \frac{e^{ik(R_{pa} - R_{qn} - R_{na})}}{R_{pa} R_{qn} R_{na}} (1 - \delta_{pa})(1 - \delta_{qn})(1 - \delta_{na}) + \text{c.c.} \right]$$

$$+ \sum_{m,n,p,q} H_{qpnm} \, e^{ik \cdot (R_{ap} - R_{aq})} \frac{e^{ik(R_{pn} + R_{na} - R_{qm} - R_{ma})}}{R_{pn} R_{na} R_{qm} R_{ma}}$$

$$\times (1 - \delta_{pn})(1 - \delta_{na})(1 - \delta_{qm})(1 - \delta_{ma}) + \ldots \Big\} . \tag{3.9}$$

Let us first consider the first, single-scattering, term on the right-hand side of (3.9). From the stationary phase argument, the integration over angles would peak at $r_0 = R_{ap} - R_{aq}$, while the integration over energies would peak at $r_0 = R_{qa} - R_{pa} > 0$. Only if these two maxima coincide we get a sizeable contribution to the integral, and this means $|R_{ap} - R_{aq}| = R_{qa} - R_{pa} > 0$ which is satisfied only if the vectors R_{ap} and R_{aq} are parallel: the atoms p and q are aligned with atom a (and the atom p lies in between a and q). Therefore, as shown in Fig. 2, we obtain a ghost image at the point x defined by $r_x = R_{ap} - R_{aq} \equiv R_q - R_p$ on the chain apq. If $q = p$ we of course get a contribution to the background at $r_0 = 0$.

Much the same can be said about the other, multiple-scattering, terms of (3.9). They all give contributions for forward scattering along chains of atoms and an enhancement of the background at $r_0 = 0$.

We see therefore that, by making a Fourier transform on the energy of the Helmholtz-Kirchhoff integral (2.25b), one is able to suppress the twin images and most of the self-hologram. As far as the latter is concerned, the only contribution left is the appearance of ghost images (i.e. false atoms) along forward scattering chains of at least three atoms.

A very good point of this procedure is that, having practically cancelled the multiple-scattering contributions, one is left only with the consideration of single scatterings (first term on the right-hand side of (3.6)).

4. Treatment of Angular Anisotropies

The angular anisotropies, arising both from the directly emitted (reference) wave and from the scattered (object) waves, lead to aberrations which include shifts of the atom positions and image distortions. As far as the scattered waves are concerned, while at low energy the atomic scattering factor is rather isotropic, as the energy increases it becomes increasingly anisotropic being very large in the forward direction.

In the literature, ways have been conceived to cope with this problem [19, 21, 24 to 28]. In these approaches the beauty of the holographic approach is a bit lost, as we shall see.

As a result of the considerations of Section 3, for the case of photoemission the image wave field is given by

$$\psi'_{\mathrm{Tobj}}(r_0) \equiv A \int_0^{+\infty} \mathrm{d}k\, w(k)\, \mathrm{e}^{ikr_0} \int_S \mathrm{d}\Omega_k\, \chi(k)\, \mathrm{e}^{-ik\cdot r_0}$$

$$\approx A \int_0^{+\infty} \mathrm{d}k\, w(k)\, \mathrm{e}^{ikr_0} \int_S \mathrm{d}\Omega_k\, \psi^*_{\mathrm{obj}}(R)\, \psi_{\mathrm{ref}}(R)\, \mathrm{e}^{-ik\cdot r_0} \tag{4.1}$$

and we can stick to single scatterings only.

The case of Auger emission will be treated here on the same basis, being understood that in the integral (4.1) one has $w(k) = \delta(k - k_f)$, where $\hbar k_f$ is the final momentum of the emitted Auger electron.

The single-scattering (SS) part of the wave function (2.10) reads

$$\psi^{\mathrm{SS}}(R) = \psi_{\mathrm{ref}}(R) + \psi^{\mathrm{SS}}_{\mathrm{obj}}(R)$$

$$= \tilde{A}\frac{\mathrm{e}^{ikR}}{R}\left\{\sum_L (-i)^l\, \mathrm{Y}_L(k)\, \mathscr{N}_{cL} + \sum_{p\neq a} \mathrm{e}^{ik\cdot R_{ap}} \sum_L O_p^L(k; R_{ap})\, \mathscr{N}_{cL}\right\}, \tag{4.2}$$

where $\tilde{A} = -m/(2\pi\hbar^2)$ and the object scattered-wave function O_p^L, and its plane wave approximation, is given by

$$O_p^L(k; R_{ap}) = \sum_{L_p} (-i)^{l_p}\, \mathrm{Y}_{L_p}(k)\, t^p_{l_p} g_{L_p L}(R_{pa}) \underset{\mathrm{PWA}}{\Rightarrow} f_p(\theta_{fpa})\frac{\mathrm{e}^{ikR_{pa}}}{R_{pa}}(-i)^l\, \mathrm{Y}_L(R_{pa}), \tag{4.3}$$

where θ_{fpa} is the angle of scattering from the atom p defined by $\cos\theta_{fpa} = k\cdot R_{pa}/kR_{pa}$.

The presence of scattering phase shifts in (4.2) (see also (4.4) and (4.5) below) is responsible for the shift in the positions of the images of the atoms.

In the case of dipole photoemission from an s-subshell, (4.2) is very simply given in the PWA,

$$\{\psi^{\mathrm{SS}}_{\text{s-subshell}}(R)\}^{\mathrm{dipole}}_{\mathrm{PWA}} = \hat{A}\mathscr{M}_{l=1}(k)\frac{\mathrm{e}^{ikR}}{R}\left\{\frac{\varepsilon\cdot k}{k} + \sum_{p\neq a}\frac{\varepsilon\cdot R_{pa}}{R_{pa}}\frac{\mathrm{e}^{i[kR_{pa}(1-\cos\theta_{fpa})+\varphi_p(\theta_{fpa})]}}{R_{pa}}|f_p(\theta_{fpa})|\right\}, \tag{4.4}$$

where $\hat{A} = em(\hbar\omega)^{1/2}/(2(2\pi)^3\,\hbar^2 k)$ is slowly energy dependent, ε and $\hbar\omega$ are the polarization unit vector and the energy of the incoming photon, and $\mathscr{M}_{l=1}(k) = \int_0^\infty r\,\mathrm{d}r\, \psi^{(+)}_{a,l=1}(k, r)\, R_{l_i=0}(r)$. We have written explicitly the amplitude $|f_p|$ and the phase φ_p of the scattering factor f_p.

In the case of Auger emission of an electron with final $L \equiv l, m$ angular momentum, in the PWA (4.2) reads

$$\{\psi^{\mathrm{SS}}_L(R)\}^{\mathrm{Auger}}_{\mathrm{PWA}}$$

$$= \hat{B}_L\frac{\mathrm{e}^{ikR}}{R}\left\{\mathrm{Y}_L(k) + \sum_{p\neq a}\frac{\mathrm{e}^{i[kR_{pa}(1-\cos\theta_{fpa})+\varphi_p(\theta_{fpa})]}}{R_{pa}}|f_p(\theta_{fpa})|\,\mathrm{Y}_L(R_{pa})\right\}, \tag{4.5}$$

where $\hat{B}_L = \hat{A}(-i)^l\,\mathscr{M}^{\mathrm{Auger}}_{cL}$.

From the structure of (4.2) we see that, if we divide the experimental photoemission anisotropy function $\chi(k)$ by the angular part of the reference wave,

$$\chi(k) \to \tilde{\chi}(k) = \frac{\chi(k)}{D_{\mathrm{ref}}(k)}, \tag{4.6a}$$

$$D_{\mathrm{ref}}(k) = \sum_L (-i)^l \, \mathrm{Y}_L(k) \, \mathcal{N}_{cL}, \tag{4.6b}$$

we eliminate altogether the distortions caused by this angular asymmetry. Note that for a dipole photoemission from an s-core level, (4.6) is tantamount to dividing by $\varepsilon \cdot k/k$, while for Auger s-wave emission the denominator $D_{\mathrm{ref}}(k)$ is of course a constant. The operation (4.6) can be considered as a redefinition of the boundary condition (2.12).

We need now to discuss how to cope with the anisotropies present in the object waves of the integrand of (4.1).

4.1 The SWEEP method

A first possible procedure is that proposed by Tong and collaborators [19, 21, 24]. To be consistent with our procedures, we shall rephrase it a bit.

We first evaluate (4.1) using the experimental $\chi(k)$ corrected as in (4.6) for the angular anisotropy of the reference wave. We then fix our attention on a particular bump p appearing at the distance R'_{ap} from the atom a and representing a neighbour of a. Pre-existing knowledge about the system in question, will avoid the risk that a self-hologram false atom of the type discussed at the end of Section 3 is taken for a good atom. We now perform the following operation on $\tilde{\chi}(k)$:

$$\tilde{\chi}(k) \to \chi_{\mathrm{SWEEP}}(k) = \frac{\tilde{\chi}(k)}{D_{\mathrm{obj}}(k; R'_{pa})}, \tag{4.7a}$$

$$D_{\mathrm{obj}}(k; R'_{pa}) = \mathrm{e}^{-ikR'_{pa}} R'_{pa} \sum_L O_p^L(k; R'_{pa}) \, \mathcal{N}_{cL} \underset{\mathrm{PWA}}{\approx} f_p(\theta_{fpa}) \sum_L (-i)^l \, \mathrm{Y}_L(R'_{pa}) \, \mathcal{N}_{cL}, \tag{4.7b}$$

and carry out the integration (4.1). In the original papers, Tong et al. actually integrate only over the forward, or backward, peak on a small angular window of half angle $\approx 30°$ centred along R'_{ap}. Their formalism is then known as the SWEEP method (for small-window energy extension process).

In (4.7), the outgoing scattered-wave function $O_p^L(k; R'_{ap})$, and the scattering factor $f_p(\theta_{fpa})$, are theoretical expressions evaluated for an atom p of a given chemical species. This second step should have yielded an improved position R''_{ap}. The procedure is repeated by dividing $\tilde{\chi}(k)$ as shown in (4.7), where now R'_{ap} is replaced by R''_{ap}. By iteration one should converge to a final value R_{ap} for the position vector of the atom p. One must repeat the same procedure also for the other bumps in order to complete the determination of the structure around the atom a.

4.2 The SWIFT method

A second procedure, proposed by Saldin and coworkers [25 to 28], is an original variation of the above approach. For coherence with the rest of our text, we discuss it within the framework of (4.1), i.e. by including also the energy Fourier transform.

After having corrected the experimental $\chi(k)$ as in (4.6) for the angular anisotropy of the reference wave, let us perform the following operation on $\tilde{\chi}(k)$ [25 to 28]:

$$\tilde{\chi}(k) \to \chi_{\text{SWIFT}}(k) = \frac{\tilde{\chi}(k)}{D_{\text{obj}}(k; r_0)}, \tag{4.8a}$$

$$D_{\text{obj}}(k; r_0) = e^{-ikr_0} r_0 \sum_L O_p^L(k; r_0)\, \mathcal{N}_{cL} \underset{\text{PWA}}{\approx} f(\theta_{f0_a}) \sum_L (-i)^l Y_L(r_0)\, \mathcal{N}_{cL}, \tag{4.8b}$$

and then carry out the integration (4.1).

Here the angle θ_{f0_a} is defined by: $\cos \theta_{f0_a} = k \cdot r_0 / k r_0$ and the outgoing scattering-wave function $O_p^L(k; r_0)$ (or the scattering factor $f(\theta_{f0_a})$) is now a generalized scattering amplitude evaluated at the position of the image point r_0 as if a hypotetical atom would be sitting there. Since the transformation involves the scattering amplitude, the authors have named it SWIFT, for scattered-wave-included Fourier transform.

According to the calculations performed in [25 to 28], with this method an improvement of the atom positions and image distortions is actually realized at the stationary-phase points $r_0 = R_{ap}$. As in the case of the SWEEP method, due care has to be applied to spot the existence of possible ghosts.

A good point of this procedure is that the entire interference pattern is inverted in only one step. No prior knowledge of the forward scattering directions locating the atoms is required. This method spoils, however, the simple structure of Fourier transform over the angles possessed by the Helmholtz-Kirchhoff algorithm (2.25b) (and also by (4.1)). as naturally obtained from the holographic approach.

Also operations (4.7) and (4.8), even within their artificiality, could be thought of as being redefinitions of the boundary condition (2.12).

5. Conclusions

In this article we have reviewed the theory of electron emission holography. Its formulation has been provided in Section 2 on a sound mathematical basis.

We have seen that, as in the optical case, one is faced with the presence of twin images. Besides, however, other artifacts appear in electron emission holography due to the fact that, at variance with the optical case, here the object wave is not small with respect to the reference wave and the scattering is in general not dominated by s-waves.

Sections 3 and 4 have been devoted to the discussion of these artifacts and to a review of the various correction procedures proposed in the literature for their elimination. In doing so, we have also seen that the proposal by Barton, Tong, and collaborators of performing an energy Fourier transform of the holography integral (2.23) is able to eliminate most of the multiple-scattering contributions to the hologram.

Apart from the complications mentioned above, the holographic method has the merit of being rather direct. One has to remember that in electron emission diffraction methods the structure information is obtained only after a lengthy trial-and-error procedure of comparing experimental spectra with those obtained by means of extensive multiple-scattering calculations. Holography requires, however, an increased amount of experimental data, and therefore of data acquisition times, with respect to the diffraction methods. But this is at hand now at the new high brightness synchrotron radiation sources.

We have seen in Section 2 that, with the use of the simple Helmholtz-Kirchoff holography integral (2.23), atoms can be located with an accuracy of a few hundredth nm at best. Taking

also into account the fact that, by performing an energy Fourier transform, one can improve this spatial resolution, we feel that, before the investigator involves himself with the more sophisticated trial-and-error method mentioned above, electron emission holography provides him with a quick tool to get within shooting range of a more accurate determination of the positions of atoms at or near a surface.

References

[1] A. SZÖKE, AIP Conf. Proc. **147**, 361 (1986).
[2] J. J. BARTON, Phys. Rev. Letters **61**, 1356 (1988).
[3] D. GABOR, Proc. Roy. Soc. A **197**, 454 (1949); Proc. Phys. Soc. B **64**, 449 (1951).
[4] S. A. CHAMBERS, Surface Sci. Rep. **16**, 261 (1992).
[5] C. S. FADLEY, Surface Sci. Rep., **19**, 231 (1993).
[6] L. FONDA, phys. stat. sol. (b) **182**, 9 (1994).
[7] B. L. GYORFFY and M. J. STOTT, Solid State Commun. **9**, 613 (1971).
[8] F. T. S. YU, Optical Information Processing, J. Wiley & Sons, New York 1983.
[9] M. BORN and E. WOLF, Principles of Optics, Pergamon Press, Oxford 1980 (p. 374).
[10] A. SOMMERFELD, Optics, Academic Press, New York/London 1964 (p. 200).
[11] C. S. FADLEY, in: Synchrotron Radiation Research: Advances in Surface and Interface Science, Vol. 1, Techniques. Ed. R. Z. BACHRACH, Plenum Press, New York 1992 (p. 421).
[12] S. THEVUTHASAN, G. S. HERMAN A. P. KADUWELA, R. S. SAIKI, Y. J. KIM, W. NIEMCZURA, M. BURGER, and C. S. FADLEY, Phys. Rev. Letters **67**, 469 (1991).
[13] P. M. LEN, S. THEVUTHASAN, C. S. FADLEY, A. P. KADUWELA, and M. A. VAN HOVE, to be published.
[14] D. K. SALDIN and P. L. DE ANDRES, Phys. Rev. Letters **64**, 1270 (1990).
[15] G. R. HARP, D. K. SALDIN, and B. P. TONNER, Phys. Rev. Letters **65**, 1012 (1990).
[16] A. P. KADUWELA, Z. WANG, M. A. VAN HOVE, and C. S. FADLEY, to be published.
[17] E. M. E. TIMMERMANS, G. T. TRAMMEL, and J. P. HANNON, J. appl. Phys. **73**, 6183 (1993).
[18] J. J. BARTON and L. J. TERMINELLO, in: Structure of Surfaces III, Ed. S. Y. TONG, M. A. VAN HOVE, X. XIDE, and K. TAKAYANAGI, Springer-Verlag, Berlin 1991 (p. 107).
[19] S. Y. TONG, HUA LI, and H. HUANG, Phys. Rev. Letters **67**, 3102 (1991).
[20] J. J. BARTON, Phys. Rev. Letters **67**, 3106 (1991).
[21] S. Y. TONG, H. HUANG, and HUA LI, Mater. Res. Soc. Symp. Proc. **208**, 13 (1991).
[22] H. HUANG, HUA LI, and S. Y. TONG, Phys. Rev. B **44**, 3240 (1991).
[23] L. J. TERMINELLO, J. J. BARTON, and D. A. LAPIANO-SMITH, J. Vacuum Sci. Technol. B **10**, 2088 (1992), Phys. Rev. Letters **70**, 599 (1993).
[24] S. Y. TONG, C. M. WEI, T. C. ZHAO, H. HUANG, and HUA LI, Phys. Rev. Letters **66**, 60 (1991).
[25] S. HARDCASTLE, Z.-L. HAN, G. R. HARP, J. ZHANG, B. L. CHEN, D. K. SALDIN, and B. P. TONNER, Surface Sci. **245**, L190 (1991).
[26] B. P. TONNER, Z.-L. HAN, G. R. HARP, and D. K. SALDIN, Phys. Rev. B **43**, 14423 (1991).
[27] D. K. SALDIN, G. R. HARP, B. L. CHEN, and B. P. TONNER, Phys. Rev. B **44**, 2480 (1991).
[28] D. K. SALDIN, G. R. HARP, and B. P. TONNER, Phys. Rev. B **45**, 9629 (1992).

(Received November 10, 1994)

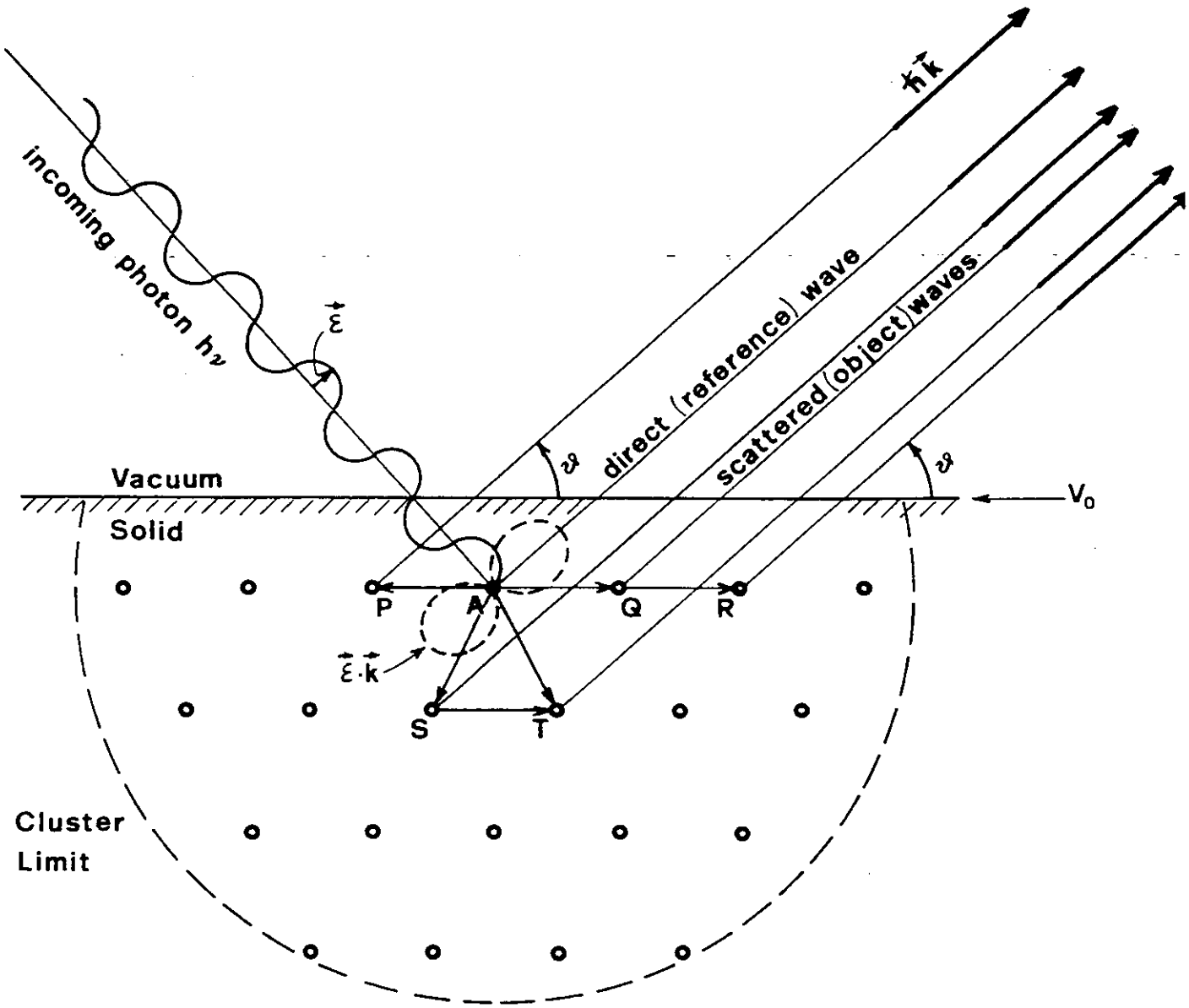
incoming photon hν
ε
ħk
direct (reference) wave
scattered (object) waves
ϑ
ϑ
Vacuum
Solid
V0
P
A
Q
R
ε·k
S
T
Cluster
Limit

Fig. 1

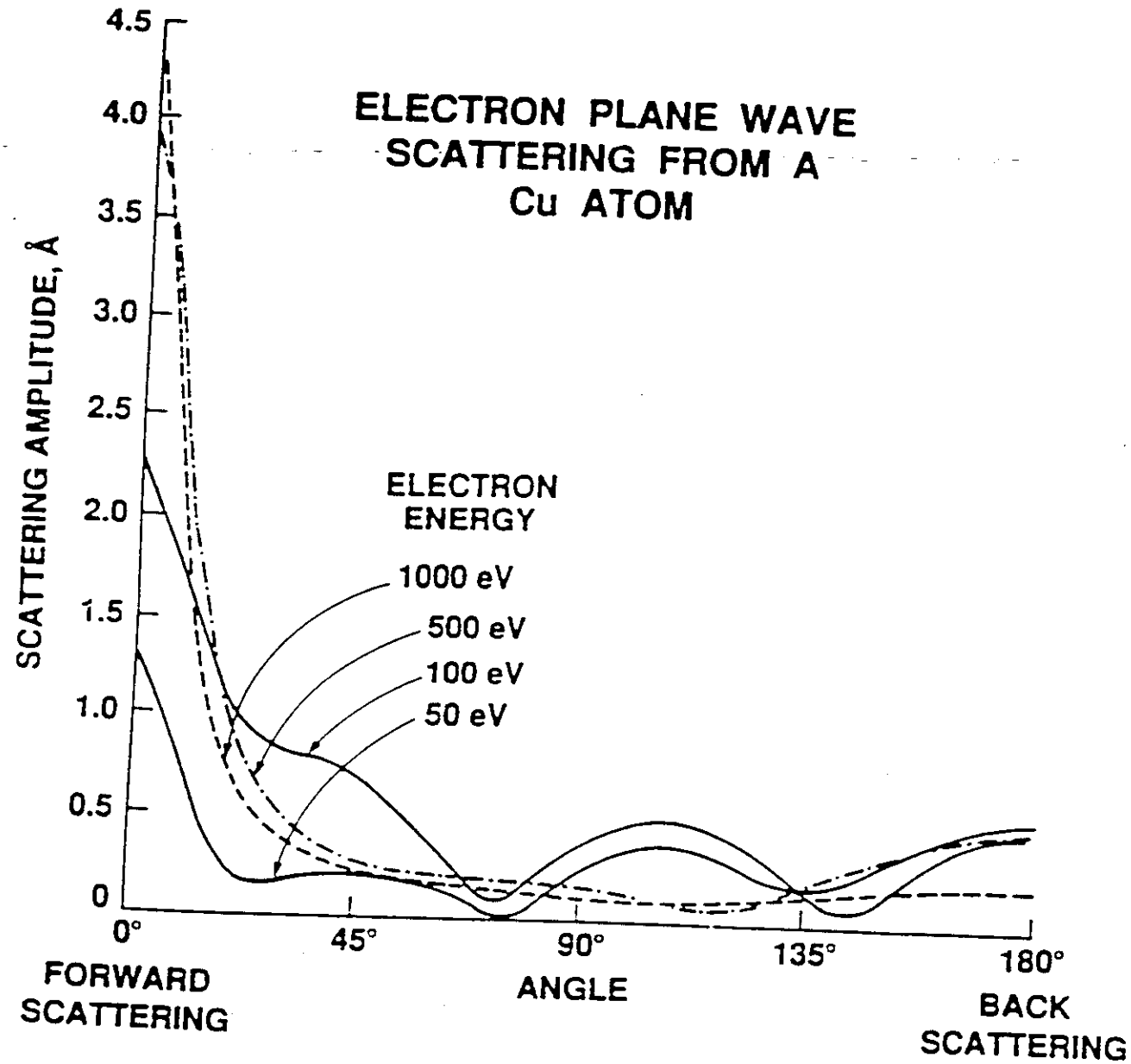
ELECTRON PLANE WAVE
SCATTERING FROM A
Cu ATOM
SCATTERING AMPLITUDE, Å
4.5
4.0
3.5
3.0
2.5
2.0
1.5
1.0
0.5
0
ELECTRON
ENERGY
1000 eV
500 eV
100 eV
50 eV
0°
45°
90°
135°
180°
FORWARD
SCATTERING
ANGLE
BACK
SCATTERING

Fig. 2

A.P. KADUWELA, D.K. SALDIN and B.P. TONNER

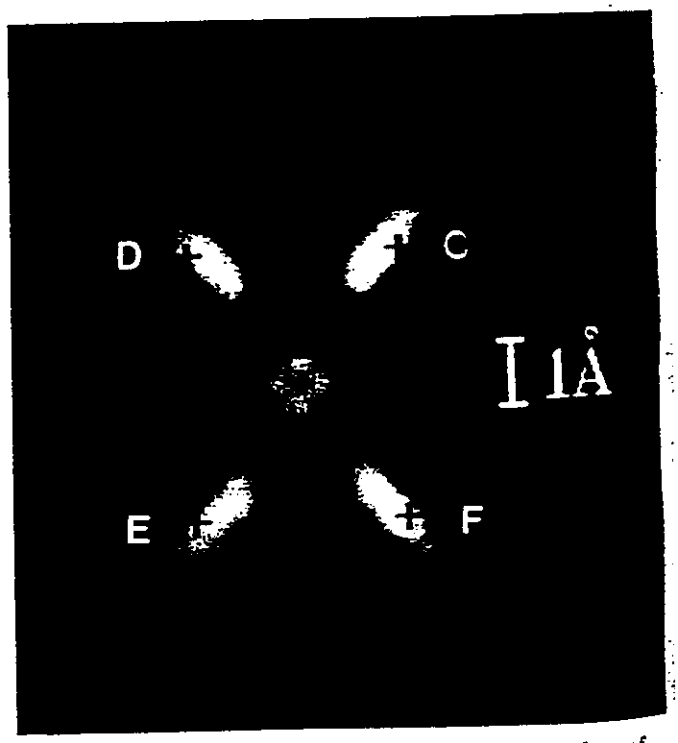

FIG. 4. A view in the plane perpendicular to the surface of the holographic reconstruction of the data from Fig. 1. The crosses mark positions of atoms in the ideal lattice. The elongated shape of the atom image is due to a reduction in resolution parallel to the electron emission direction.

Phys. Rev. Letters 65, 1012 (1990)

PETERSEN, TERMINELLO, BARTON and SHIRLEY

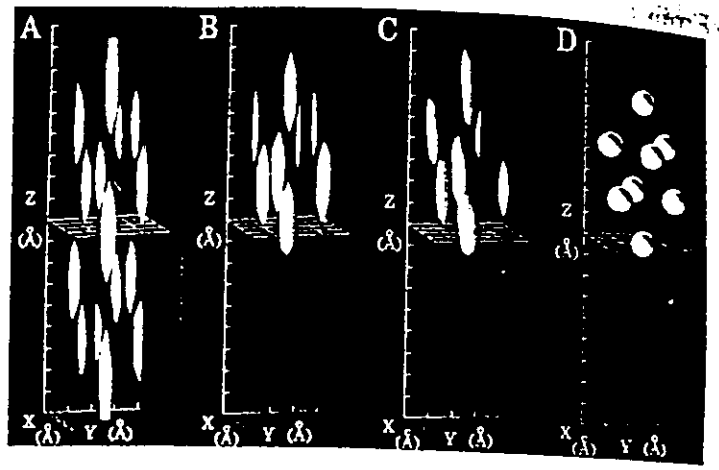

Fig. 10. Elimination of twin images as a result of the application of energy FT holography. Panel A shows a symmetry-averaged $\chi(k)$ at $k = 9.8$ Å^{-1} (366 eV). Twin images appear for $z < 0$. Panel B shows the result of phase-summing on eight values of k in the interval 8.8–10.2 Å^{-1}. Panel C shows the same pattern without symmetry averaging. Panel D represents a model showing the atoms in the positions as expected. (From Ref. 89.)

- Chem. Phys. Lett. 213, 412(1993); 220, 46 (1994).